Published in final edited form as:
Nature. 2020 December 01; 588(7836): 146–150. doi:10.1038/s41586-020-2600-6.

Association of COVID-19 inflammation with activation of the C5a-C5aR1 axis

Julien Carvelli[#1,2], **Olivier Demaria**[#3], **Frédéric Vély**[#4,5], **Luciana Batista**[3], **Nassima Chouaki Benmansour**[6,10], **Joanna Fares**[3], **Sabrina Carpentier**[3], **Marie-Laure Thibult**[3], **Ariane Morel**[3], **Romain Remark**[3], **Pascale André**[3], **Agnès Represa**[3], **Christelle Piperoglou**[4,5], **the Explore COVID-19 IPH group**
Laura Assante Miranda, William Baron, Nourhène Belaid, Clarisse Caillet, Flavien Caraguel, Barbara Carrette, Florent Carrette, Fabien Chanuc, Rachel Courtois, Aurore Fenis, Marilyn Giordano, Mathilde Girard-Madoux, Marc Giraudon-Paoli, Nicolas Gourdin, Gwendoline Grondin, Franceline Guillot, Guillaume Habif, Solène Jaubert, Julie Lopez, Mélanie Le Van, Naouel Lovera, Marine Mansuy, Elodie Bonnet, Audrey Sansaloni, Annick Reboul, Emmanuel Mitry, Camille Nekkar-Constant, Valentine Péri, Paul Ricaut, Léa Simon, Jean-Baptiste Vallier, Marie Vétizou, Robert Zerbib
Innate Pharma

[3], **the Explore COVID-19 Marseille Immunopole group**
Sophie Ugolini, Marion Etiennot, Justine Galluso
Ciml

Luc Lyonnet, Jean-Marie Forel, Laurent Papazian, Lionel Velly, Baptiste André, Antoine Briantais, Benoit Faucher, Estelle Jean, Julie Seguier, Veronique Veit, Jean-Robert Harlé, Boris Pastorino, Clémence Delteil, Laurent Daniel
AP-HM

Jean-Paul Boudsocq, Axelle Clerc, Emmanuel Delmond, Pierre-Olivier Vidal, Hélène Savini
Hôpital d'Instruction des Armées Laveran

Bruno Coutard
AMU, UVE-UMR190, Inserm 1207, IHU Méditerranée Infection, Marseille, France

* vivier@ciml.univ-mrs.fr.

Author contributions: J.C, F.V. and E.V initiated and designed the research. O.D and E.V. wrote the manuscript with the help of other coauthors. O.D., L.B., J.F. S.C., M-L.T., A.M., P.A., C.P., L.L., W.B., N.B., C.C., B.C., F.C., R.C., A.F., M.G., M.G-M., M.G-P., N.G., G.G., F.G., S.J., J.L., M. L-V., N.L., M.M., C.N-C., V.P., A.R., P.R., J-B.V., M.V., E.B., A.S., A.R., Y.M., E.M., R.Z., L.L., J.G., M.Et., G.H., R.R., L.S., F.C., L.A.M., S.U., B.P., B.C., C.D., L.D. performed the experiments and analyzed and/or interpreted results. J-M.F, L.P., L.V., B.A., A.B., B.F., E.J, J.S., V.V., J-R.H., J.P.B., A.C., E.D., P-O.V., H.S., J.C., N.C.B, M. G., J-M.F., L.P., M.Eb. and N.S. were in charge of patient care and contributed to the discussion of the results. L.B., N.C.B., J.F., S.C., M-L.T. and A.M. equally contributed.

Competing interests: O.D., L.B., J.F., S.C., M.-L.T., A.M., R.R., P.A., A.Represa, L.A.M., W.B., N.B., C.C., F. Caraguel, B.Carrette, F.Carrette, F.Chanuc, R.C., A.F., M.Giordano, M.G.-M., M.G.-P., N.G., G.G., F.G., G.H., S.J., J.L., M.L.V., N.L., M.M., E.B., A.S., A.Reboul, E.M., C.N.-C., V.P., P.R., L.S., J.-B.V., M.V., R.Z., Y.M. and E.V. are employees of Innate Pharma. The other authors declare no competing interests.

Europe PMC Funders Author Manuscripts

[2,4,6,10], **Pierre Yves Cordier**[6], **Erwan Le Dault**[6], **Christophe Guervilly**[2,7], **Pierre Simeone**[2,8], **Marc Gainnier**[1,2], **Yannis Morel**[3], **Mikael Ebbo**[4,9], **Nicolas Schleinitz**[4,9], **Eric Vivier**[3,4,5,*]

[1]Assistance Publique des Hôpitaux de Marseille, Hôpital de la Timone, Réanimation des Urgences, France

[2]Aix Marseille Univ, Marseille, France

[3]Innate Pharma, Marseille, France

[4]Aix Marseille Univ, CNRS, INSERM, CIML, Marseille, France

[5]Assistance Publique des Hôpitaux de Marseille, Hôpital de la Timone, Immunology, Marseille Immunopole, France

[6]Hôpital d'Instruction des Armées Laveran, Marseille, France

[7]Assistance Publique des Hôpitaux de Marseille, Hôpital Nord, Réanimation des Détresses, Respiratoires et Infections Sévères, Aix-Marseille Université, Marseille, France

[8]Assistance Publique des Hôpitaux de Marseille, Hôpital de la Timone, Réanimation Polyvalente, Aix-Marseille Université, Marseille, France

[9]Assistance Publique des Hôpitaux de Marseille, Hôpital de la Timone, Internal Medicine, France

[10]Assistance Publique des Hôpitaux de Marseille, Marseille, France

[#] These authors contributed equally to this work.

Abstract

Coronavirus disease 2019 (COVID-19) is a new pandemic disease caused by infection with severe acute respiratory syndrome coronavirus 2 (SARS-CoV-2). The C5a anaphylatoxin and its receptor C5aR1 (CD88) play a key role in the initiation and maintenance of several inflammatory responses, by recruiting and activating neutrophils and monocytes in the lungs[1]. We provide a longitudinal analysis of immune responses, including immune cell phenotyping and assessments of the soluble factors present in the blood and broncho-alveolar lavage fluid (BALF) of patients at various stages of COVID-19 severity: paucisymptomatic, pneumonia and acute respiratory distress syndrome (ARDS). We report an increase in soluble C5a levels proportional to COVID-19 severity and high levels of C5aR1 expression in blood and pulmonary myeloid cells, supporting a role for the C5a-C5aR1 axis in the pathophysiology of ARDS. Anti-C5aR1 therapeutic monoclonal antibodies (mAbs) prevented C5a-mediated human myeloid cell recruitment and activation, and inhibited acute lung injury (ALI) in human C5aR1 knockin mice. These results suggest that C5a-C5aR1 axis blockade might be used as a means of limiting myeloid cell infiltration in damaged organs and preventing the excessive lung inflammation and endothelialitis associated with ARDS in COVID-19 patients.

Most COVID-19 patients present only a few mild symptoms, but about 15% of patients progress to severe pneumonia, and about 5% develop ARDS, for which effective therapeutic strategies are urgently required[2]. The immune system plays a dual role in COVID-19, contributing to both virus elimination and ARDS development[2]. A detailed characterization of the immune responses occurring during disease progression from mild to severe forms is

thus crucial to an understanding of the ways in which we could manipulate immunity to propose new therapies. In particular, given the urgent need for effective treatments for pneumonia in COVID-19 patients, dissection of the immune responses occurring during the course of COVID-19 could lead to the repurposing of approved immunomodulatory drugs and candidate drugs already tested in clinical trials. We thus monitored immune parameters in a cohort of 82 individuals: 10 healthy controls (HC), 10 paucisymptomatic (pauci) COVID-19 patients, 34 patients with pneumonia (pneumo) and 28 patients with ARDS due to SARS-CoV-2 (Supplementary Table 1). We focused on molecular pathways that could block the overt inflammation associated with ARDS.

Disease severity was associated with an increase in the amounts of plasma C-reactive protein (CRP) and inflammatory cytokines, such as interleukin-6 (IL-6), and the chemokines CCL4 (macrophage inflammatory protein-1β), CCL2 (monocyte chemoattractant protein 1) and CXCL9 (monokine induced by gamma interferon), produced by and acting on myeloid cells (Fig. 1a). These results confirmed earlier observations on the “cytokine storm” that develops in patients with severe COVID-19[3]. The ability of plasma from patients to neutralize SARS-CoV-2 virus is also correlated with disease severity (Extended Fig. 1a), consistent with previous data reporting higher titers of anti-SARS-CoV-2 antibodies in patients with severe COVID-19[4].

We decided to focus on the complement factor C5a, which mediates strong chemoattraction and the activation of myeloid cells[5], and plays well-documented roles specifically in lung inflammation and injury[6]. The complement cascade plays a crucial role in pathogen sensing and clearance, and inflammation[7], and involves several components, including cell surface receptors and soluble regulators. In the final phase of the response, the membrane attack complex (MAC: C5b9), and the potent chemoattractants and inflammatory mediators C3a and C5a are generated. The MAC forms transmembrane channels on the surface of pathogen cells, disrupting the cell membrane and leading to cell death. The C3a and C5a proteins regulate inflammation by binding to their receptors, C3aR and C5aR1[8]. Exaggerated complement activation contributes to the pathogenesis of many inflammatory and immune diseases[5]. Many studies of the lung epithelium have reported depositions of complement components during inflammation and suggested that the systemic activation of complement leads, via C5a, to neutrophil recruitment, activation, and adhesion to the pulmonary endothelium, resulting in cell damage, and subsequent ALI and ARDS, which may be fatal[6,1,9]. We observed an increase in plasma C5a levels proportional to COVID-19 severity (Fig. 1b). C5a levels increased in a few patients in the paucisymptomatic group, and was significantly higher than those in HC in both groups displaying lung damage: the pneumonia and ARDS groups (Fig. 1b). The longitudinal follow-up of COVID-19 patients revealed that the upregulation of circulating C5a levels was maintained for at least 10 days after the inclusion of the patients in our cohort (Extended Fig. 1b). The higher levels of C5a in the patients with the most severe symptoms suggests a role for this anaphylatoxin in the cytokine storm occurring in patients developing ARDS. Increased systemic and local complement pathway activity was confirmed by transcriptomic analysis on the peripheral blood of COVID-19 patients, showing an upregulation of *C1Q* and *C2* expression (Extended Fig. 1c) and by the presence of C5b9, as shown by immunostaining, in lung sections from COVID-19 patients (Extended Fig. 1d). Consistent with these results, high levels of C5a in

COVID-19 patients have recently been reported to be a consequence of overt activation of the complement cascade by the SARS-CoV-2 N-protein[10]. Furthermore, anti-SARS-CoV-2 antibodies[4] and CRP may also contribute to the activation of the classical pathway of complement during COVID-19. Thus, factors triggering activation of the lectin and the classical complement pathway are upregulated in COVID-19 and may sustain the high level of C5a detected.

We found that COVID-19 was associated with peripheral blood neutrophilia (Fig. 2a), as reported in other cohorts[11]. No major changes were observed in the total peripheral blood monocyte population, but the proportion of conventional $CD14^{+}CD16^{-}$ monocytes increased, whereas the proportion of inflammatory $CD14^{low}CD16^{+}$ monocytes decreased in peripheral blood (Fig. 2b), consistent with the possibility of inflammatory monocytes leaving the bloodstream and homing to tissues. This hypothesis was supported by transcriptomic analyses on symptomatic COVID-19 patients, which revealed not only an increase in transcript levels of genes including *IRAK3*, *MS4A6A*, *CD33*, *CD300C*, *VCAN*, *CD1D*, *CCR1*, *OAS1*, *CD163* and *C3AR1* in peripheral blood monocytes, but also an upregulation of macrophage and monocyte transcriptomic signatures in inflamed lungs (Extended Fig. 1c).

Both circulating neutrophils and monocytes displayed strong C5aR1 expression in healthy individuals that was also observed in the various groups of COVID-19 patients (Fig. 2c). Longitudinal immune-monitoring follow-up of patients with pneumonia and ARDS showed that the levels of C5aR1 molecules remained stable on circulating neutrophils and monocytes, or even increased during the course of the disease (Extended Fig. 2a). Consistent with the inflammatory function of C5a[12], and the expression of C5aR1 on monocytes, C5a increased the production of the inflammatory cytokines IL-6, TNFα and CCL2 induced by LPS on purified blood monocytes isolated from the various groups of COVID-19 patients (Fig. 2d). C5a also increased the production of cytokines by the monocytes of COVID-19 patients following stimulation with R848, which activates the TLR7/TLR8 MyD88-dependent signaling pathway, mimicking the single-stranded RNA of SARS-CoV-2 (Fig. 2d).

Given that severe COVID-19 is associated with lung disease, we then focused on this organ. C5a was detected in the BALF of ARDS COVID-19 patients (Fig. 3a). Inflammatory cytokines, such as CXCL8, CXCL9, CCL2, and, to a lesser extent, CCL4, IL-6, TNF-α and IL-1β, were also detected in these samples (Fig. 3a). Large numbers of neutrophils and monocytes were found in the BALF of ARDS COVID-19 patients and these cells expressed C5aR1 (Fig. 3b). In addition, the analysis of single-cell RNAseq data from healthy controls and ARDS COVID-19 patients[13] revealed major changes in the myeloid cell population infiltrating the lungs during the course of SARS-CoV-2 infection. Indeed, the major myeloid cell subset (subset A) in healthy controls and the major myeloid cell subset (subset B) in ARDS COVID-19 patients were clearly different (Fig. 3c and Extended Fig. 3a and 3b). The cells of subset B were characterized by higher levels of transcripts for inflammatory cytokine genes, such as *CXCL8*, *CCL2*, *CCL4*, *CXCL9*, *TNF*-α and *IL-6* (Fig. 3d). A slight upregulation was observed in subset B, but both myeloid cell subsets expressed *C5aR1* (Fig. 3d). A multiplex immunohistochemistry analysis of lungs from deceased ARDS COVID-19

patients confirmed pulmonary infiltration with $CD68^+CD163^+$ macrophages, a substantial proportion of which expressed C5aR1 (Extended Fig. 3c; right panel), relative to lung tissue from a control without COVID-19 (Extended Fig. 3c; left panel). It is becoming increasingly clear that severe COVID-19 is associated with the spread of the virus through the epithelial barrier and endothelialitis[14,15]. We observed obliterating endarteritis associated with an accumulation of $C5aR1^+$ macrophages around the arteries and in the thrombus (Extended Fig. 3d). Together with the high levels of C5a in symptomatic COVID-19 patients, these data support the hypothesis that C5a production leads to the chemo-attraction and activation of myeloid cells in the lungs, and contributes to the overt release of inflammatory cytokines. As C5a can also promote the secretion of CCL2, a strong chemoattractant for monocytes, C5a may also promote the recruitment of inflammatory cells indirectly, through the induction of other chemokines. It is also possible that the vasculitis associated with severe COVID-19 is linked to the production of C5a, as other types of vasculitis, such as anti-neutrophil cytoplasmic antibody (ANCA)-associated vasculitis, are mediated by C5a[16].

Based on this hypothesis, we reasoned that C5a-C5aR1 axis blockade could be proposed as a potential therapeutic strategy for severe COVID-19. Several molecules could be repurposed to this end, including anti-C5 mAbs, anti-C5a mAbs and C5aR1 antagonists. We focused on avdoralimab, a fully human Fc-silent mAb against C5aR1 that prevents its binding to C5a. *In vitro*, C5aR1 blockade with avdoralimab inhibited C5a-induced neutrophil activation, as shown by evaluation of the induction of CD11b expression at the cell surface (Fig. 4a). The C5a-mediated upregulation of CD11b was also inhibited by other C5aR1 antagonists or anti-C5a mAbs (Extended Fig. 4a). Avdoralimab blocked the neutrophil activation induced by very high concentrations of C5a (Fig. 4b). Concerning the infiltration of $C5aR1^+$ myeloid cells in the inflamed lungs of patients with severe COVID-19, avdoralimab also inhibited the C5a-induced migration of neutrophils *in vitro* (Fig. 4c). We then investigated whether avdoralimab could block the development of ALI in a mouse model. As avdoralimab targets human C5aR1, we used mice with a knock in for human C5aR1 (HuC5aR1 KI mice)[18] displaying huC5aR1 expression exclusively on $CD11b^+$ myeloid cells (Extended Fig. 4b). HuC5aR1 KI mice receiving an intranasal instillation of recombinant human C5a developed acute lung inflammation and injury 18 hours post injection, as shown by the infiltration of $CD45^+$ immune cells including $Ly6G^+Ly6C^+$ neutrophils and $Ly6G^-Ly6C^+$ monocytes into the lung (Fig. 4d) and the release of albumin in BALF (Fig. 4e), a marker of alveolar-capillary permeability and lung injury. ALI was confirmed by histopathology analysis of lung sections that revealed massive inflammatory cell infiltration, alveolar hemorrhage and thickening of alveolar walls in lungs of C5a-treated mice (Extended Fig. 4c), as previously described[9]. Avdoralimab blocked the infiltration of both cell types (Fig. 4d), prevented albumin release in BALF (Fig. 4e) and limited C5a-induced ALI histopathological features (Extended Fig. 4c). Finally, avdoralimab also inhibited the increase in IL-6, TNF and CCL2 secretion induced *in vitro* by C5a in monocytes purified from COVID-19 patients and activated with a single strand RNA virus-like stimulus (Fig. 4f). Avdoralimab appears, thus, suitable for blocking the C5a-C5aR1 axis, which is active during COVID-19. The high levels of C5a observed in COVID-19 do not appear to be a passenger phenomenon, as preliminary efficacy data reported two COVID-19 patients recovering from ARDS following treatment with an anti-C5a blocking mAb (IFX-1)[10]. Furthermore, four patients with severe

COVID-19 treated with an anti-C5 mAb (eculizumab), exhibited a drop in circulating inflammatory markers[17]. There are several advantages to blocking C5aR1 rather than other components of the complement cascade. First, blocking C5a or C5aR1 leaves C5b intact and preserves the MAC, which plays a key role in controlling several infections. A loss of the MAC would raise safety concerns in COVID-19, as symptomatic patients often develop comorbid conditions, such as bacterial infections, for which the MAC is required. Second, C5aR1 blockade has the advantage over C5a blockade of having no effect on the second C5a receptor, C5L2. The function of C5L2 remains elusive, but it has been suggested that it can act as a decoy receptor, with anti-inflammatory roles[19].

Our data, highlighting the role of the C5a-C5aR1 axis in the pathogenesis of severe COVID-19, are consistent with several previous observations. Indeed, high C5a levels have also been described in various preclinical models of acute lung disease due to highly pathogenic viruses, such as SARS-CoV-1, H1N1, H5N1 and H7N9[1]. High levels of C5a have also been found in the upper respiratory tract and in serum samples from patients infected with the H1N1 virus[20]. Furthermore, BALF from ARDS patients was found to display robust C5a-dependent chemotactic activity[21]. In a mouse model of MERS-CoV infection, C5a concentrations were high in serum samples and lung tissues[22], and anti-C5aR1 antibody treatment decreased viral replication in lung tissue[22]. In a green monkey model of H7N9 infection, treatment with an anti-C5a antibody significantly decreased the levels of IL-6, IFN-γ, TNF and IL-1β and neutrophil infiltration into the lungs[23]. Overall, C5a inhibition markedly decreased the ALI and systemic inflammation induced by viral infection[24].

In addition, the complement system links innate immunity to coagulation[25,26], and its overactivation could promote thrombotic events in patients with severe COVID-19[27]. Complement blockade may, therefore, prevent thrombosis in affected individuals. Further evidence for the involvement of the complement system in the pathogenesis of severe COVID-19 is also provided by the existence of genetic variants of complement regulatory proteins, such as C1 inhibitor (C1inh) and CD55[28]. C1inh bridges the gap between the complement system and the kallikrein-kinin pathway, which is also activated in COVID-19. In severe COVID-19, SARS-CoV-2 saturates the ACE2 receptors expressed in human airway epithelium[29], resulting in an excess of angiotensin II[30], which, in turn, leads to an excess of kallikrein-kinin that may contribute to tissue injury[30] and the activation of coagulation through the contact system[26]. C1inh downregulates these pathways, but could be overwhelmed by the kinin excess and complement cascade overactivity observed in response to SARS-CoV-2.

The data presented here support a role of the C5a-C5aR1 axis in inflammatory mechanisms underlying ARDS development in patients at early or late stages of SARS-COV-2 infection. As described above, in addition to pneumonia and ARDS, there are data to suggest a role of C5a in other COVID-19-related symptoms, including heart, kidney or endothelial cell dysfunction[14], providing support for the testing of C5a-C5aR1 axis blockade in COVID-19 patients. We suggest that such a blockade may prevent the transition from a localized epithelial disease (non-severe COVID-19) to a diffuse endothelial disease (severe COVID-19) (Extended Figure 4d).

Europe PMC Funders Author Manuscripts

Methods

Study subjects and clinical considerations

Over a period of one month (03-27-2020 to 04-24-2020), 82 subjects were recruited from three hospitals (Timone and Nord University Hospitals and Laveran Military Hospital, Marseille). Twenty-eight of these patients were on mechanical ventilation for COVID-19-related-ARDS (P/F ratio < 300) (ARDS group), 34 patients required oxygen support at a rate of less than 5 L/min for COVID-19-related pneumonia (pneumonia group). Ten patients had a paucisymptomatic form of COVID-19 compatible with outpatient care (paucisymptomatic group). COVID-19 was diagnosed on the basis of positive SARS-CoV-2 RT-PCR on nasopharyngeal samples and/or typical CT-scan findings[31]. We also included 10 healthy volunteers (control group), with no fever or symptoms in the days before sampling and negative for SARS-CoV-2 RT-PCR. The characteristics of the patients are presented in Supplementary Table 1. Biological samples were first collected within three days of diagnosis and the start of care (T0: < 72 h, early time-point). When possible, the next two time-points for sample collection were located between days 5 and 10 (T1: D5 to D10, intermediate time-point) and after day 10 (T2: > D10, late time-point). Flow cytometry analyses were performed on fresh blood samples (EDTA tubes) and BALFs, immediately after collection. Clinical progression was evaluated between the early and intermediate time points and between the intermediate and late time points. A favorable outcome was defined as weaning from mechanical ventilation (ARDS group) or oxygen support (pneumonia group). Death or multiple organ failure (ARDS group) and admission to the ICU (pneumonia group) were considered unfavorable outcomes. In other cases, patients were considered to be stable.

Ethics approval statement

All the patients (and/or initially their families) provided written informed consent before sampling and for the use of their clinical and biological data. The study protocol was approved on 03-27-2020 by the Committee for the Protection of Persons Ile-de-France III – France (#2020-A00757-32). The pathological examination used in this study was performed secondary to a medical autopsy following COVID-19 related-death, with family agreement and notified to the representative of the Commission on Data Processing and Freedom (MR003 research).

Animals

C57Bl/6J female mice were purchased at Janvier Labs and used between 8 to 12 weeks old. HuC5aR1 KI mice were bred at Charles River Laboratories under specific pathogen-free conditions. Female mice were used at eight to 12 weeks of age and were allowed to acclimate to the housing facility for at least one week. All animal experiments were performed in accordance with the rules of the Innate Pharma ethics committee and were approved by the Ministère de l'Enseignement Supérieur, de la Recherche et de l'Innovation – France (APAFIS#25418-2020051512242806 v2).

Reagent list

DPBS (1X) (14190-094, Gibco); RPMI medium 1640 (1X) (31870-025, Gibco); Sodium pyruvate 100 mM (100X) (11360-039, Gibco); L-glutamine 200 mM (100X) (25030-024, Gibco); Minimum essential medium non-essential amino acids solution (11140-035, Gibco); Trypan blue stain (0.4%) (15250-061, Gibco); Ficoll-Paque PLUS (17-1440-03, GE Healthcare); Fetal bovine serum (F7524, Sigma); Dimethyl sulfoxide (D2650-100ML, Sigma); CD14 microbeads human (130-050-201, Miltenyi); EasySep direct human neutrophil isolation kit (19666, Stemcell); Bovine serum albumin (A9418-100G, Sigma); UltraPure 0.5 M EDTA, pH 8.0 (15575-038, Invitrogen); LPS EK ultrapure (tlrl-peklps, Invivogen); R848 (tlrl-r848, Invivogen); C5a (IPH 1D9 batch 1A, Innate Pharma); C5a (2037-C5-025, R&D Systems); Avdoralimab (Innate Pharma), Isotypic control (Fc-silent hIgG1) (Innate Pharma); CD33-PECF594 clone WM53 (562492, BD Biosciences); CD19-PECy7 clone SJ25C1(557835, BD Biosciences); CD3-BUV496 clone UCHT1 (564809/612940, BD Biosciences); CD15-BV510 clone W6D3 (563141, BD Biosciences); CD45-BV711 clone HI30 (564357, BD Biosciences); CD16-BUV395 clone 3G8 (563785, BD Biosciences); CD14-BUV737 clone M5E2 (564444/612763, BD Biosciences); HLA-DR-AF700 clone L243 (307626, BioLegend); LIVE DEAD NEAR IR (L34976, ThermoFisher); Mouse serum (015-000-120, Jackson ImmunoResearch); CD88 C5aR PE clone S5/1 (344304, BioLegend); Anti-CD16 FITC (556616, BD Biosciences); Anti-CD11b PE-Cy5 (555389, BD Biosciences); U-PLEX kit (N05235A-1, MSD); OptEIATM huC5a ELISA (557965, BD Biosciences); Mouse Albumin ELISA Kit (E99-134, Bethyl Laboratories); Ficoll (11778538, Invitrogen); Dextran (31382, Sigma); Calcein AM (C3100MP, Invitrogen); Fibrinogen (F3879, Sigma); Transwell Fluoroblok 3 μm insert (351151, Corning); EDTA (15575-038, Invitrogen); Sodium azide (71290-100g, Sigma); Optilyse C solution (A11895, Beckman Coulter); CytoFix (554655, BD Bioscience); Avacopan (HY-17627, Clinisciences); Anti-C5a (Innate Pharma); Anti-mouse Ly-6C BV510 clone HK1.4 (128033, BioLegend); Anti-mouse Ly-6G BV786 clone 1A8 (740953, BD Biosciences); Anti-mouse CD45 BUV395 clone 30F11 (564279, BD Biosciences), Anti-mouse CD11b BUV737 clone M1/70 (564443/612800, BD Biosciences); Anti-mouse C5aR1-APC clone 20/70 (130-106-124, Miltenyi Biotec); Anti-human CD88 clone S5/1 (HM2094-100UG, Hycult Biotech); Anti-human CD68 clone KP1 (M0814, Agilent); Anti-human CD163 clone EDHu-1 (MCA1853, BioRad).

SARS-CoV-2 detection by PCR

SARS-CoV-2 RNA was detected by real-time reverse transcription-PCR, as previously described[32].

Seroneutralization assay

Experiments were performed in BSL3 facilities with a clinical isolate of SARS-CoV-2. Virus neutralization tests (VNTs) were performed as previously described[33]. Briefly, VNTs were performed in a 96-well plate, with Vero-E6 cells and a SARS-CoV-2 strain (Ref-SKU:026V-03883 isolated at Charité University, Berlin, Germany; EVA-GLOBAL H2020 project; Grant Agreement 871029). Two-fold serial dilutions of serum samples (final serum dilutions of 1/20 to 1/160) were mixed with 100 $TCID_{50}$ of SARS-CoV2 and dispensed on

the confluent cell monolayer. The plates were incubated for four days and examined for the presence (no neutralization) or absence (neutralization) of CPE under an inverted microscope.

Preparation of PBMCs and plasma

Whole blood collected in EDTA tubes was pooled and diluted 1/2 in PBS. PBMCs were isolated by centrifugation on a Ficoll gradient, and 10^7 PBMCs per vial were frozen in freezing medium (90% FCS + 10% DMSO). Plasma was collected from the upper phase of the Ficoll gradient, aliquoted and used for the quantification of soluble factors.

Soluble factor assessment

Human IL-6, CXCL9, CCL2, CCL4, CXCL8, TNF-α and IL-1β levels were analyzed with the U-PLEX kit supplied by MSD (U-PLEX 10-Assay, 96-Well SECTOR Plate, ref: N05235A-1), according to the manufacturer's instructions. The U-PLEX plate was loaded into an MSD instrument to measure the intensity of emitted light, which is proportional to the amount of analyte present in the sample. Circulating C5a-desArg levels were analyzed with the BD OptEIATM huC5a ELISA test. Mouse albumin in BALF was analysed by ELISA (Bethyl). HRP-conjugated secondary Ab was detected by incubation with a peroxidase substrate solution (TMB), and the reaction was stopped by acidification. Plates were read at 450 nm.

Flow cytometry

Blood collected into EDTA tubes was washed in PBS before staining with LiveDead (Thermo Fisher) according to the manufacturer's instructions. Cells were incubated with mouse serum to saturate the Fc receptors, and were then incubated with the appropriate antibody cocktail. Red blood cells were lysed in Optilyse C Solution (Beckman Coulter), according to the manufacturer's instructions. Cells were fixed in Cell Fix solution (BD), according to the manufacturer's instructions. Data were acquired in an LSRFortessaX20 flow cytometer. The FCS3.0 files obtained were exported from BD FACSDiva software and imported into FlowJo v.10.5.2 (BD Biosciences). Automated compensation was calculated with FACSDiva software and single-stained compensation beads. This compensation matrix was analyzed in detail in FlowJo, by investigating the N-by-N view feature and the pairwise expression of all proteins stained in this study. Fluorescence minus one (FMO) experiments were run before this study, to facilitate optimization of the compensation matrix. We then adjusted the compensation matrix where necessary due to over- or under-compensation by the automatic algorithm.

Immune cell counts

Absolute counts per μL of blood were determined with BD TBNK Trucount™ Tubes. Absolute counts for a particular cell population (A) were obtained by dividing the number of positive cell events (X) by the number of bead events (Y), and then multiplying by the BD Trucount bead concentration (N/V, where N = number of beads per test* and V = test volume). A = X/Y × N/V. The number of positive counts for neutrophils and monocytes was established with the $CD45^+SSC^{high}$ and $CD45^+SSC^{int}$ gating strategies, respectively.

C5a inhibitors

Avdoralimab is a fully human mutated Fc-silent IgG1 mAb against C5aR1 (US 2020/0017599A1). Anti-C5a mAb is a chimeric mutated Fc silent IgG1 isotype cloned from the sequences of mouse anti-huC5a INab308 (WO2015/140304A1), showing the same variable sequences as IFX-1. C5aR1 antagonist (avacopan) was purchased from Clinisciences (HY-17627).

Neutrophil migration

Neutrophils were isolated from fresh blood by sedimentation in 6% dextran to separate plasma and leukocytes, followed by centrifugation on a Ficoll density gradient. The pellet, containing neutrophils, was recovered, and the red blood cells were lysed by incubation in 0.2% NaCl. Osmotic balance was restored by adding an equal volume of 1.6% NaCl. Isolated neutrophils were loaded with 10 μM calcein AM. Cell density was adjusted before the addition of avdoralimab or its isotype control at a final concentration of 10 μg/mL. Neutrophils were dispensed into the top chamber of a fibrinogen- and BSA-coated Transwell Fluoroblok 3 μm insert. The lower chamber was filled with RPMI 1640 with or without 3 nM C5a (R&D Systems,) and the same antibody was added to the top chamber (avdoralimab, isotype control or PBS). After 30 minutes of incubation at +37 ± 1°C under an atmosphere containing 5 ± 1% CO_2, images of the lower face of the inserts were acquired on a Biotek Cytation 5 plate-reading microscope, and analyzed with Halo software (Indica Labs), using the CytoNuclear FL module to count the cells that had crossed the membrane.

Neutrophil activation

Various concentrations of avdoralimab were added to the blood samples in culture-treated 96-well U-bottom plates, and incubated for 20 min at 37°C under an atmosphere containing 5% CO_2. We then added 18 nM human recombinant C5a (R&D Systems) to the samples. Plates were incubated for 20 minutes at 37°C under an atmosphere containing 5% CO_2. Samples were then stained for flow cytometry analysis with anti-CD16 FITC and anti-CD11b PE-Cy5 antibodies. Erythrocytes were lysed with Optilyse C solution (Beckman Coulter, A11895), according to the manufacturer's protocol, and resuspended in CytoFix (BD Bioscience 554655) for fixation. Cells were then analyzed on a FACS Canto II flow cytometer (BD Biosciences) with FACS Diva software.

Monocyte activation

Monocytes were purified with the $CD14^+$ selection kit (Miltenyi). We used 30 000 monocytes to seed 96-well U-bottom plates. Cells were activated by overnight incubation with R848 (50 ng/mL), LPS (0.5 ng/mL) and C5a (1 μg/mL; IPH). In some conditions, monocytes were incubated with avdoralimab (IPH, 20 μg/mL) or its isotype control (IPH, 20 μg/mL) for 30 minutes before stimulation. IL-6, TNF-α and CCL2 were quantified in the supernatant.

Mouse model of lung inflammation

Isoflurane-anesthetized huC5aR1 KI mice received 3.1 μg of recombinant huC5a (R&D) in 40 μL phosphate-buffered saline (PBS), by intranasal instillation. After 18 hours, mice were

killed with a lethal dose of ketamine/xylazine cocktail (ketamine 300 mg/kg; xylazine 30 mg/kg). The lungs were flushed with 2 mL 2 mM EDTA in PBS to obtain BALF. After centrifugation (300 × *g*, 5 min, 4°C), BALF cells were counted and stained for flow cytometry analysis with anti-CD45, anti-Ly6C, anti-Ly6G and anti-CD11b antibodies. For histology analysis, 18 hours after intranasal instillation of huC5a, lungs were fixed in formalin, dissected, embedded in paraffin and sectioned to 5-μm. Sections were dewaxed and stained with hematoxylin and eosin. Slides were finally scanned using a Nanozoomer S60 (Hamamatsu) and examined for evidence of lung damage.

Multiplex immunohistochemistry (OPAL™) staining protocol, image acquisition and data analysis

Multiplexed IHC was performed with a Leica Bond Rx on 5 μm-thick formalin-fixed paraffin-embedded lung tissue sections from individuals with and without COVID-19. Consecutive staining was performed by heat-induced antigen retrieval followed by incubation with primary antibody (anti-C5aR1 clone S5/1 at 1 μg/mL). The signal was amplified and detected with Opal™ polymer horseradish peroxidase and Opal 520 (Akoya Biosciences). The sections were then subjected to heat-induced antibody stripping and incubated with the next antibody (anti-CD163 clone EDHu-1 at 1 μg/mL, detected with Opal 620, and, finally, anti-CD68 clone KP1 at 0.1 μg/mL, detected with Opal 690) and spectral DAPI. All Opal reagents were used at a dilution of 1/150. Slides were finally mounted in ProLong Diamond antifade mounting medium (Thermo Fisher) and scanned with a Vectra Polaris (Akoya Biosciences). Hematoxylin and eosin-stained slides were scanned with a Nanozoomer (Hamamatsu). After spectral deconvolution and whole-slide reconstruction of the multiplexed IHC stained sections, digital pathology methods were used to determine the density of positive cells. All analyses were performed with Halo (Indica Labs) and R.

Transcriptomic analysis

Transcriptomic analyses were performed on previously reported data[34,13]. The RNASeq data for two BALF samples from patients (each in duplicate), three PBMC samples from healthy controls and three PBMC samples from patients were downloaded from the National Genomics Data Center (https://bigd.big.ac.cn/) under accession number PRJCA002326. The RNA-seq data for three BALF samples from healthy controls were downloaded from the SRA database under accession numbers: SRR10571724, SRR10571730, and SRR10571732.

RNASeq pipeline: The reads were mapped to human genome (hg38) release 96 from Ensembl with STAR[68]. PCR replicates mapping to the human genome were removed with the Picard MarkDuplicates program (Broad Institute 2019, http://broadinstitute.github.io/picard/). Gene expression was calculated with featureCounts in the SubReads package (v1.6.4)[36]. TPM (transcripts per million) values were calculated from the raw counts and $\log_2$-transformed. The depth of sequencing of the patient BALF samples was low (< 1 M).

Batch effect correction: we corrected for the batch effect between the datasets for BALF samples from healthy donors and those from patients and PBMC samples with Combat[37], using the model: ~ Batch + Status (Patient or Healthy) + Sample Type (PMBC or BALF). An analysis of differential expression between PBMC samples from healthy donors and

Europe PMC Funders Author Manuscripts

those from patients was performed on raw counts with DESeq2[38]. Significance was defined as an adjusted *p*-value <0.05. The metagene *IRAK3, MS4A6A, CD33, CD300C, VCAN, CD1D, CCR1, OAS1, CD163, CD14, FCN1, AIF1, PLA2G7* was used to calculate the macrophage and monocyte transcriptomic signature. The significance of the difference between healthy donors and patients was evaluated in a Wilcoxon test. The single-cell RNASeq data for 12 BALF samples from three healthy donors, three patients with mild COVID-19 and six patients with severe COVID-19 were downloaded from the Gene Expression Omnibus (GEO) database (http://www. https://www.ncbi.nlm.nih.gov/geo) under accession number GSE145926. Quality controls were applied to each cell, for all samples, with the same criteria as for the initial analysis: gene number between 200 and 6,000, UMI count > 1,000 and mitochondrial gene percentage < 0.1, with the Seurat package (v3.1.0). After filtering, 63740 cells were validated. As previously described by Liao et al., the filtered gene-barcode matrix was first normalized with 'LogNormalize' methods in Seurat v.3, with default parameters. The top 2,000 variable genes were then identified by the 'vst' method with the Seurat FindVariableFeatures function. The variables 'nCount_RNA' and 'percent.mito' were regressed out in the scaling step and PCA was performed on the top 2,000 variable genes. For the re-analysis presented here, the batch effects across different donors were removed by Harmony[39] and UMAP was performed on the top 50 dimensions for visualizing the cells. Graph-based clustering was performed on the Harmony corrected data, with a resolution of 1.2, and defined major clusters composed of epithelial cells, B and plasma cells, T and NK cells, dendritic cells, monocytes, macrophages and neutrophils. The 50610 myeloid cells were re-integrated and reclustered.

Data analysis and statistics

All statistical analyses were performed with R (version 3.6.1). The ggpubr (version 0.2.5) and lmerTest (version 3.1.2) packages were used for statistical tests. The gtsummary package (version 1.3.0) was used for the clinical table. The sva package (version 3.32.1) was used to correct the batch effect of RNAseq. Packages ggplot2(version 3.2.1) and pheatmap (1.0.12) were used for the graphical representations of RNASeq analyses. The Seurat package (version 3.1.0) was used for all analyses of single-cell RNASeq. For the comparison of groups at timepoint T0, *p*-values were obtained for two-tailed Wilcoxon rank-sum tests. For longitudinal analysis in the pneumonia group, the *p*-values for comparisons of T1 and T0 were obtained in two-tailed Wilcoxon signed-rank tests. No statistical tests were performed for T2 in this group. For the ARDS group, a mixed model was computed, with timepoint as a fixed effect (categorical variable) and patient as a random effect. Confidence intervals and *p*-values were based on the *t*-distribution, with degrees of freedom according to the Kenward-Roger method, and the normality of residuals was verified. Plots were drawn with GraphPad Prism version 8.1.1. Boxplots represent the median and 25th to 75th percentiles and the whiskers denote the maximum and minimum values.

Europe PMC Funders Author Manuscripts

Extended Data

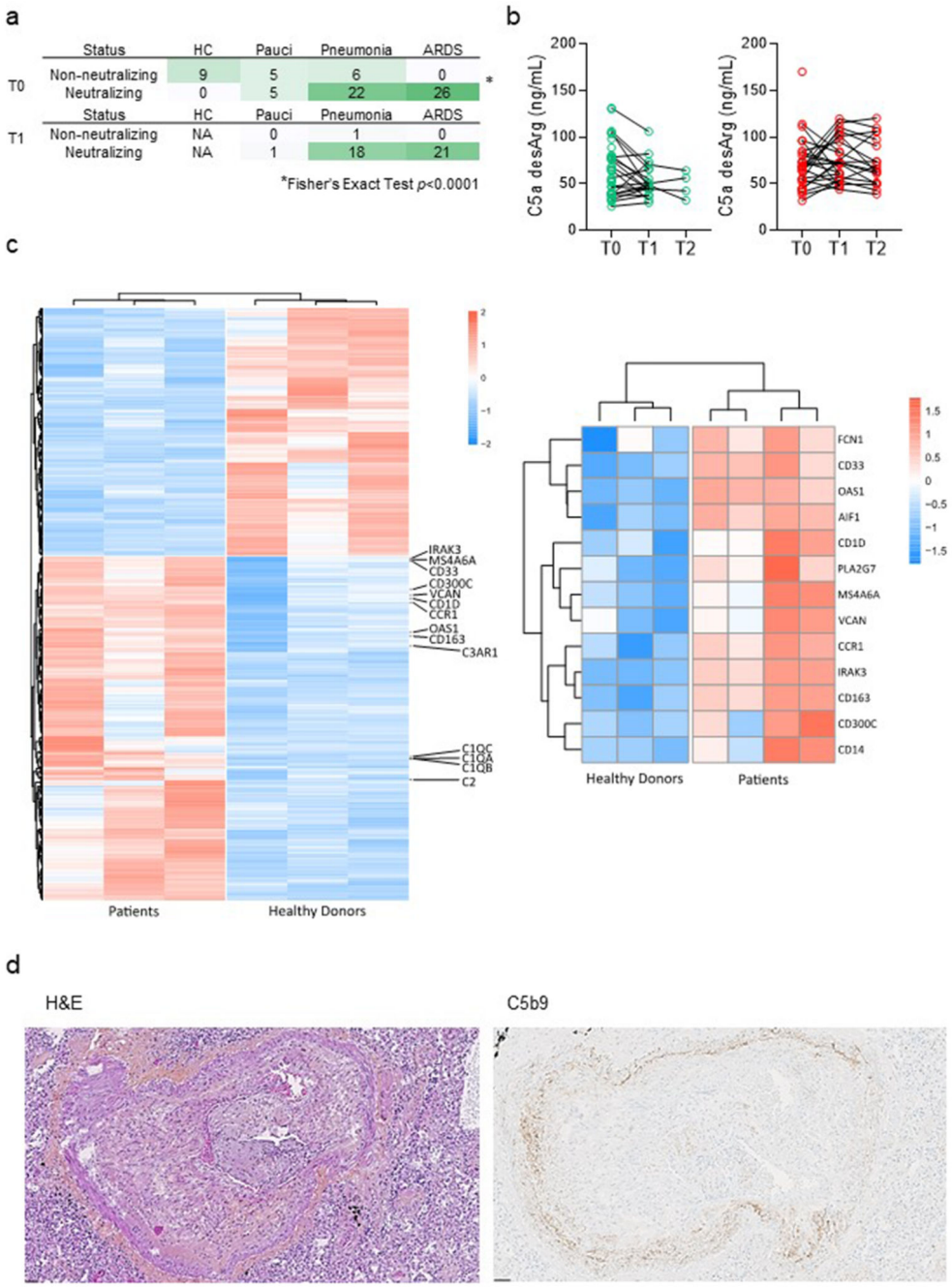

Extended Fig. 1. Immune activation in COVID-19 patients.

a, Number of patients for each level of disease severity, classified according to SARS-CoV-2 seroneutralizing status. Biological samples were collected at T0: < 72 h after the start of hospital care; T1: between days 5 and 10. **b**, Concentration of C5a desArg in plasma from pneumonia and ARDS patients followed over time. T0: < 72 h after the beginning of hospital care; T1: between days 5 and 10; T2: > day 10. *p*-values for the comparison of T1 (n=19) and T0 (n=34) in pneumonia group were obtained using two-tailed Wilcoxon signed-

rank tests. No statistical tests were performed for T2 (n=4). For ARDS group, a mixed model was computed with timepoint (categorical variable) as a fixed effect and patient as a random effect. n=28 for T0, n=23 for T1 and n=18 for T2. Confidence intervals and *p*-values are based on the *t*-distribution, with degrees of freedom according to the Kenward-Roger method. Each symbol represents a single donor. **c,** Left, Heatmap of genes differentially expressed (logFC >2 & FDR < 5%) between PBMC samples from healthy donors and COVID-19 patients. Right, Heatmap of monocyte and macrophage metagene expression in lung samples from healthy donors and COVID-19 patients. **d**, Three lung samples from deceased patients were obtained and suitable for IHC analysis. Left, H&E staining of obliterating endarteritis lesions in the lungs of a representative COVID-19 patient. Right, C5b9 IHC staining on lung sections of a representative COVID-19 patients, demonstrating complement pathway activation in lung. Scale bar = 50 μm.

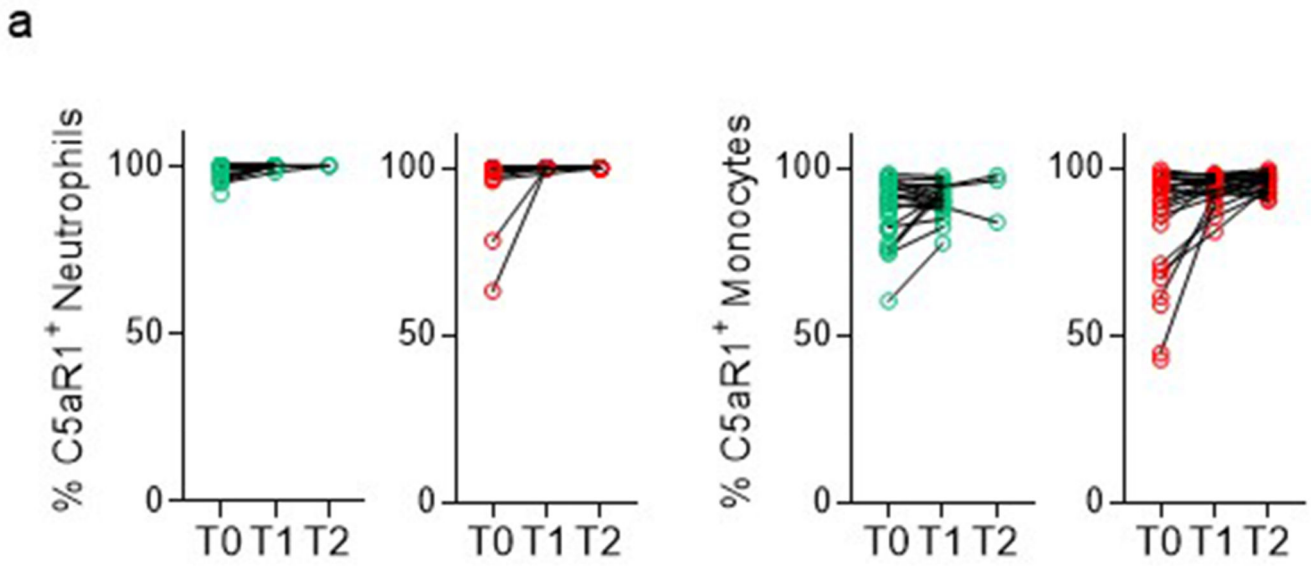

Extended Fig. 2. C5aR1 expression remained stable on myeloid cells during the course of COVID-19.

a, % C5aR1-expressing neutrophils and monocytes in pneumonia (green) and ARDS (red) patients followed over time. T0: < 72 h after the start of hospital care; T1: between days 5 and 10; T2: > day 10. For pneumonia group, n= 34 for T0, n=18 (neutrophils) and 21 (monocytes) for T1 and n= 3 for T2. For ARDS group, n=28 for T0, n= 23 for T1 and n= 22 for T2. Each symbol represents a single donor.

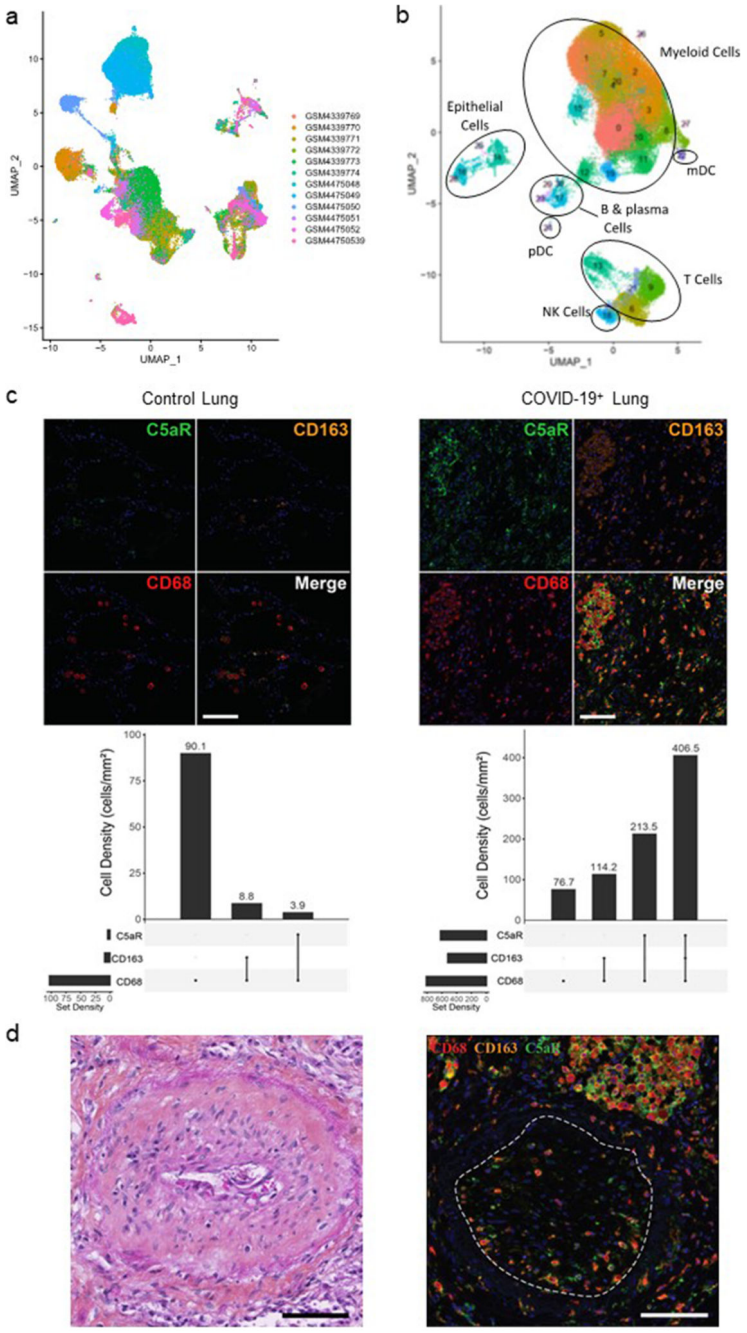

Extended Fig. 3. Myeloid cell analysis in COVID-19 patients.

a-b, Integration of transcriptomic single-cell data with Harmony**. a,** UMAP projection of donors before integration. **b**, UMAP projection of major cell types and associated clusters after integration by Harmony. **c,** Representative multiplexed IHC staining of C5aR (green), CD68 (red) and CD163 (orange) on lung sections from control or COVID-19 patients among three samples from deceased patients and suitable for IHC analyses. Scale 100 μm. Quantifications represent cell density per mm^2 of multiplexed IHC staining of C5aR1, CD68 and CD163. **d**, Three samples from deceased patients were obtained and suitable for IHC

analysis. Endoarteritis lesions were observed in two out of three patients, consistent with previous reports. The patient without endoarteritis lesions did not die from COVID-19. Left, representative H&E staining of obliterating endarteritis lesions in the lungs of COVID-19 patients. Right, representative multiplexed IHC staining of C5aR1 (green), CD68 (red) and CD163 (orange) showing that obliterating endarteritis was frequently associated with C5aR1^{+} macrophages surrounding the arteries and in the thrombus (white dotted line). Scale 100 μm.

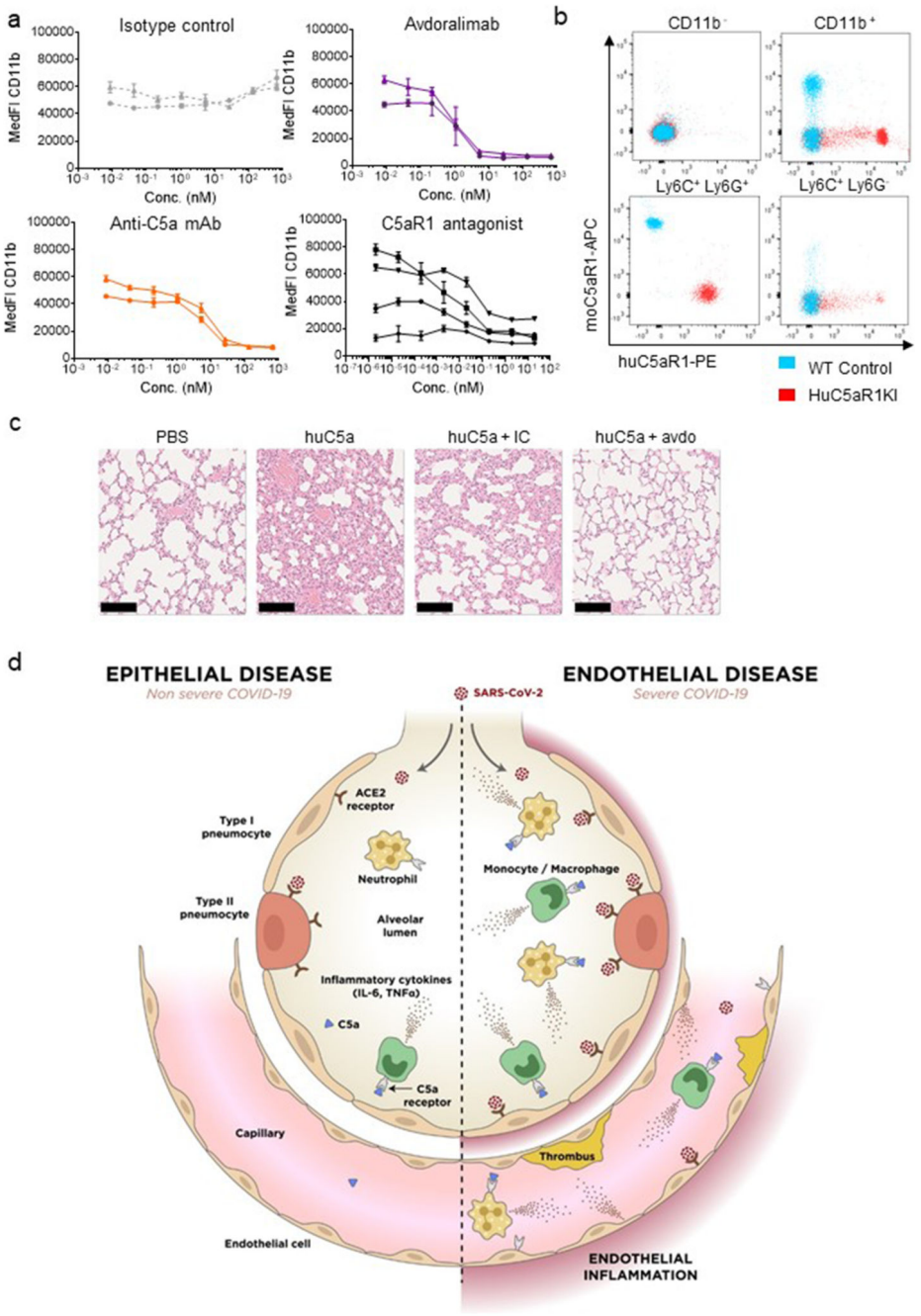

Europe PMC Funders Author Manuscripts

Extended Fig. 4. Targeting C5aR1 to block C5a-mediated myeloid cell activation.

a, Analysis of the efficacy of increasing doses of avdoralimab (purple), an anti-C5a mAb (orange), a C5aR1 antagonist (avacopan, black) or IC (gray) for blocking C5a-induced CD11b upregulation on human neutrophils. Each line represents data from a single donor +/− SD from experimental duplicates (PBS) or triplicates (inhibitors). **b**, Comparative expression of mouse C5aR1 (moC5aR1) and human C5aR1 (huC5aR1) on $CD11b^-$ non-myeloid cells, $CD11b^+$ myeloid cells, including $Ly6C^+Ly6G^+$ neutrophils and $Ly6C^+Ly6G^-$ monocytes, from WT (blue) and huC5aR1 KI (red) mice. **c,** H&E staining of lungs from huC5aR1 KI mice treated intranasally with huC5a. Mice were pretreated with avdoralimab (avdo) or isotype control (IC), when indicated. Scale bar =100 μm. Pictures are representative of 2 independent experiments. **d,** A model of C5a involvement in COVID-19: SARS-CoV-2 infects the human airway epithelium via the ACE2 receptors located principally on type II pneumocytes. Left, in non-severe COVID-19, the infection remains confined to the epithelium (epithelial disease), thanks to the efficient action of the immune system. C5a allows the recruitment of myeloid cells without triggering an inflammatory storm, and the virus is eliminated. Right, in severe COVID-19, SARS-CoV-2 escapes the immune system, crosses the epithelium and infect endothelial cells (endothelial disease). The myeloid cells recruited by C5a and endothelial cells release large amounts of inflammatory cytokines. The COVID-19-related cytokine storm and endothelialitis-associated microthrombosis are triggered. The patient's condition worsens and the virus can infect other organs.

Supplementary Material

Refer to Web version on PubMed Central for supplementary material.

Authors

Julien Carvelli[#1,2], **Olivier Demaria**[#3], **Frédéric Vély**[#4,5], **Luciana Batista**[3], **Nassima Chouaki Benmansour**[6,10], **Joanna Fares**[3], **Sabrina Carpentier**[3], **Marie-Laure Thibult**[3], **Ariane Morel**[3], **Romain Remark**[3], **Pascale André**[3], **Agnès Represa**[3], **Christelle Piperoglou**[4,5], **the Explore COVID-19 IPH group**
Laura Assante Miranda, William Baron, Nourhène Belaid, Clarisse Caillet, Flavien Caraguel, Barbara Carrette, Florent Carrette, Fabien Chanuc, Rachel Courtois, Aurore Fenis, Marilyn Giordano, Mathilde Girard-Madoux, Marc Giraudon-Paoli, Nicolas Gourdin, Gwendoline Grondin, Franceline Guillot, Guillaume Habif, Solène Jaubert, Julie Lopez, Mélanie Le Van, Naouel Lovera, Marine Mansuy, Elodie Bonnet, Audrey Sansaloni, Annick Reboul, Emmanuel Mitry, Camille Nekkar-Constant, Valentine Péri, Paul Ricaut, Léa Simon, Jean-Baptiste Vallier, Marie Vétizou, Robert Zerbib
Innate Pharma

[3], **the Explore COVID-19 Marseille Immunopole group**
Sophie Ugolini, Marion Etiennot, Justine Galluso
Ciml

Luc Lyonnet, Jean-Marie Forel, Laurent Papazian, Lionel Velly, Baptiste André, Antoine Briantais, Benoit Faucher, Estelle Jean, Julie Seguier, Veronique Veit, Jean-Robert Harlé, Boris Pastorino, Clémence Delteil, Laurent Daniel
AP-HM

Jean-Paul Boudsocq, Axelle Clerc, Emmanuel Delmond, Pierre-Olivier Vidal, Hélène Savini
Hôpital d'Instruction des Armées Laveran

Bruno Coutard
AMU, UVE-UMR190, Inserm 1207, IHU Méditerranée Infection, Marseille, France

[2,4,6,10], **Pierre Yves Cordier**[6], **Erwan Le Dault**[6], **Christophe Guervilly**[2,7], **Pierre Simeone**[2,8], **Marc Gainnier**[1,2], **Yannis Morel**[3], **Mikael Ebbo**[4,9], **Nicolas Schleinitz**[4,9], **Eric Vivier**[3,4,5,*]

Laura Assante Miranda, **William Baron**, **Nourhène Belaid**, **Clarisse Caillet**, **Flavien Caraguel**, **Barbara Carrette**, **Florent Carrette**, **Fabien Chanuc**, **Rachel Courtois**, **Aurore Fenis**, **Marilyn Giordano**, **Mathilde Girard-Madoux**, **Marc Giraudon-Paoli**, **Nicolas Gourdin**, **Gwendoline Grondin**, **Franceline Guillot**, **Guillaume Habif**, **Solène Jaubert**, **Julie Lopez**, **Mélanie Le Van**, **Naouel Lovera**, **Marine Mansuy**, **Elodie Bonnet**, **Audrey Sansaloni**, **Annick Reboul**, **Emmanuel Mitry**, **Camille Nekkar-Constant**, **Valentine Péri**, **Paul Ricaut**, **Léa Simon**, **Jean-Baptiste Vallier**, **Marie Vétizou**, **Robert Zerbib**

Sophie Ugolini, **Marion Etiennot**, **Justine Galluso**

Luc Lyonnet, **Jean-Marie Forel**, **Laurent Papazian**, **Lionel Velly**, **Baptiste André**, **Antoine Briantais**, **Benoit Faucher**, **Estelle Jean**, **Julie Seguier**, **Veronique Veit**, **Jean-Robert Harlé**, **Boris Pastorino**, **Clémence Delteil**, **Laurent Daniel**

Jean-Paul Boudsocq, **Axelle Clerc**, **Emmanuel Delmond**, **Pierre-Olivier Vidal**, **Hélène Savini**

Bruno Coutard

Affiliations

Innate Pharma

Ciml

AP-HM

Hôpital d'Instruction des Armées Laveran

AMU, UVE-UMR190, Inserm 1207, IHU Méditerranée Infection, Marseille, France

[1]Assistance Publique des Hôpitaux de Marseille, Hôpital de la Timone, Réanimation des Urgences, France

[2]Aix Marseille Univ, Marseille, France

[3]Innate Pharma, Marseille, France

[4]Aix Marseille Univ, CNRS, INSERM, CIML, Marseille, France

[5]Assistance Publique des Hôpitaux de Marseille, Hôpital de la Timone, Immunology, Marseille Immunopole, France

[6]Hôpital d'Instruction des Armées Laveran, Marseille, France

[7]Assistance Publique des Hôpitaux de Marseille, Hôpital Nord, Réanimation des Détresses, Respiratoires et Infections Sévères, Aix-Marseille Université, Marseille, France

[8]Assistance Publique des Hôpitaux de Marseille, Hôpital de la Timone, Réanimation Polyvalente, Aix-Marseille Université, Marseille, France

[9]Assistance Publique des Hôpitaux de Marseille, Hôpital de la Timone, Internal Medicine, France

[10]Assistance Publique des Hôpitaux de Marseille, Marseille, France

Acknowledgements

We thank all the healthcare workers involved in the analysis, diagnosis and treatment of patients at AP-HM and Hôpital Laveran, especially Elise Kaspi, Eric Garnotel, Corinne Surcouf, Francois Xavier Le Flem (Bataillon des Marins Pompiers Marseille). We thank all our patients, supporters and families for their confidence in our work. The E.V. laboratory at CIML and Assistance-Publique des Hôpitaux de Marseille is supported by funding from the European Research Council (ERC) under the European Union's Horizon 2020 research and innovation program (TILC, grant agreement No. 694502 and MInfla-TILC, grant agreement No. 875102 - MInfla-Tilc), the *Agence Nationale de la Recherche* including the PIONEER Project (ANR-17-RHUS-0007), MSDAvenir, Innate Pharma and institutional grants awarded to the CIML (INSERM, CNRS, and Aix-Marseille University) and Marseille Immunopole.

Data availability

The RNASeq data for two BALF samples from patients (each in duplicate), three PBMC samples from healthy controls and three PBMC samples from patients were downloaded from the National Genomics Data Center (https://bigd.big.ac.cn/) under accession number PRJCA002326. The RNA-seq data for three BALF samples from healthy controls were downloaded from the SRA database under accession numbers: SRR10571724, SRR10571730, and SRR10571732. The single-cell RNASeq data is available from the Gene Expression Omnibus (GEO) database (https://www.ncbi.nlm.nih.gov/geo) under accession number GSE145926. Requests for additional materials or data can be made via email to the corresponding author.

References

1. Wang R, Xiao H, Guo R, Li Y, Shen B. The role of C5a in acute lung injury induced by highly pathogenic viral infections. Emerging microbes & infections. 2015; 4:e28.doi: 10.1038/emi.2015.28 [PubMed: 26060601]
2. Cao X. COVID-19: immunopathology and its implications for therapy. Nature reviews Immunology. 2020; 20:269–270. DOI: 10.1038/s41577-020-0308-3
3. Mehta P, et al. COVID-19: consider cytokine storm syndromes and immunosuppression. Lancet. 2020; 395:1033–1034. DOI: 10.1016/S0140-6736(20)30628-0 [PubMed: 32192578]
4. Long QX, et al. Antibody responses to SARS-CoV-2 in patients with COVID-19. Nature medicine. 2020; doi: 10.1038/s41591-020-0897-1

5. Guo RF, Ward PA. Role of C5a in inflammatory responses. Annual review of immunology. 2005; 23:821–852. DOI: 10.1146/annurev.immunol.23.021704.115835
6. Bosmann M, Ward PA. Role of C3, C5 and anaphylatoxin receptors in acute lung injury and in sepsis. Adv Exp Med Biol. 2012; 946:147–159. DOI: 10.1007/978-1-4614-0106-3_9 [PubMed: 21948367]
7. Ricklin D, Hajishengallis G, Yang K, Lambris JD. Complement: a key system for immune surveillance and homeostasis. Nature immunology. 2010; 11:785–797. DOI: 10.1038/ni.1923 [PubMed: 20720586]
8. Guo RF, Riedemann NC, Ward PA. Role of C5a-C5aR interaction in sepsis. Shock. 2004; 21:1–7. DOI: 10.1097/01.shk.0000105502.75189.5e
9. Russkamp NF, et al. Experimental design of complement component 5a-induced acute lung injury (C5a-ALI): a role of CC-chemokine receptor type 5 during immune activation by anaphylatoxin. FASEB J. 2015; 29:3762–3772. DOI: 10.1096/fj.15-271635 [PubMed: 25999468]
10. Gao T, et al. Highly pathogenic coronavirus N protein aggravates lung injury by MASP-2-mediated complement over-activation. medRxiv. 2020; doi: 10.1101/2020.03.29.20041962
11. Liu J, et al. Neutrophil-to-Lymphocyte Ratio Predicts Severe Illness Patients with 2019 Novel Coronavirus in the Early Stage. medRxiv. 2020; doi: 10.1101/2020.02.10.20021584
12. Riedemann NC, et al. Increased C5a receptor expression in sepsis. The Journal of clinical investigation. 2002; 110:101–108. DOI: 10.1172/JCI15409 [PubMed: 12093893]
13. Liao M, et al. Single-cell landscape of bronchoalveolar immune cells in patients with COVID-19. Nature medicine. 2020; doi: 10.1038/s41591-020-0901-9
14. Varga Z, et al. Endothelial cell infection and endotheliitis in COVID-19. Lancet. 2020; 395:1417–1418. DOI: 10.1016/S0140-6736(20)30937-5 [PubMed: 32325026]
15. Teuwen LA, Geldhof V, Pasut A, Carmeliet P. COVID-19: the vasculature unleashed. Nature reviews Immunology. 2020; doi: 10.1038/s41577-020-0343-0
16. Jayne DRW, et al. Randomized Trial of C5a Receptor Inhibitor Avacopan in ANCA-Associated Vasculitis. Journal of the American Society of Nephrology: JASN. 2017; 28:2756–2767. DOI: 10.1681/ASN.2016111179 [PubMed: 28400446]
17. Diurno F, et al. Eculizumab treatment in patients with COVID-19: preliminary results from real life ASL Napoli 2 Nord experience. European review for medical and pharmacological sciences. 2020; 24:4040–4047. DOI: 10.26355/eurrev_202004_20875 [PubMed: 32329881]
18. Lee H, et al. Human C5aR knock-in mice facilitate the production and assessment of anti-inflammatory monoclonal antibodies. Nature biotechnology. 2006; 24:1279–1284. DOI: 10.1038/nbt1248
19. Gerard NP, et al. An anti-inflammatory function for the complement anaphylatoxin C5a-binding protein, C5L2. J Biol Chem. 2005; 280:39677–39680. DOI: 10.1074/jbc.C500287200 [PubMed: 16204243]
20. Bjornson AB, Mellencamp MA, Schiff GM. Complement is activated in the upper respiratory tract during influenza virus infection. Am Rev Respir Dis. 1991; 143:1062–1066. DOI: 10.1164/ajrccm/143.5_Pt_1.1062 [PubMed: 2024815]
21. Trujillo G, et al. Cofactor regulation of C5a chemotactic activity in physiological fluids. Requirement for the vitamin D binding protein, thrombospondin-1 and its receptors. Molecular immunology. 2011; 49(3):495–503. DOI: 10.1016/j.molimm.2011.09.024 [PubMed: 22014686]
22. Jiang Y, et al. Blockade of the C5a-C5aR axis alleviates lung damage in hDPP4-transgenic mice infected with MERS-CoV. Emerging microbes & infections. 2018; 7:77.doi: 10.1038/s41426-018-0063-8 [PubMed: 29691378]
23. Sun S, et al. Treatment with anti-C5a antibody improves the outcome of H7N9 virus infection in African green monkeys. Clinical infectious diseases. 2015; 60:586–595. DOI: 10.1093/cid/ciu887 [PubMed: 25433014]
24. Sun S, et al. Inhibition of complement activation alleviates acute lung injury induced by highly pathogenic avian influenza H5N1 virus infection. American journal of respiratory cell and molecular biology. 2013; 49:221–230. DOI: 10.1165/rcmb.2012-0428OC [PubMed: 23526211]

25. Foley JH. Examining coagulation-complement crosstalk: complement activation and thrombosis. Thrombosis research. 2016; 141(Suppl 2):S50–54. DOI: 10.1016/S0049-3848(16)30365-6 [PubMed: 27207425]
26. Thomson TMTE, Casis E, Paciucci R. C1-INH and the Contact System in COVID-19-Associated Coagulopathy. Preprints. 2020; doi: 10.20944/preprints202005.0262.v1
27. Magro C, et al. Complement associated microvascular injury and thrombosis in the pathogenesis of severe COVID-19 infection: A report of five cases. Translational Research. 2020; doi: 10.1016/j.trsl.2020.04.007
28. Ramlall V, Thangaraj P, Tatonetti NP, Shapira SD. Identification of Immune complement function as a determinant of adverse SARS-CoV-2 infection outcome. medRxiv. 2020; doi: 10.1101/2020.05.05.20092452
29. Zhang H, et al. Expression of the SARS-CoV-2 ACE2 Receptor in the Human Airway Epithelium. American journal of respiratory and critical care medicine. 2020; doi: 10.1164/rccm.202003-0541OC
30. Kuba K, et al. A crucial role of angiotensin converting enzyme 2 (ACE2) in SARS coronavirus-induced lung injury. Nature medicine. 2005; 11:875–879. DOI: 10.1038/nm1267
31. Ai T, et al. Correlation of Chest CT and RT-PCR Testing in Coronavirus Disease 2019 (COVID-19) in China: A Report of 1014 Cases. Radiology. 2020; doi: 10.1148/radiol.2020200642
32. Amrane S, et al. Rapid viral diagnosis and ambulatory management of suspected COVID-19 cases presenting at the infectious diseases referral hospital in Marseille, France, - January 31st to March 1st, 2020: A respiratory virus snapshot. Travel Med Infect Dis. 2020; doi: 10.1016/j.tmaid.2020.101632
33. Nurtop E, et al. Combination of ELISA screening and seroneutralisation tests to expedite Zika virus seroprevalence studies. Virology journal. 2018; 15:192.doi: 10.1186/s12985-018-1105-5 [PubMed: 30587193]
34. Xiong Y, et al. Transcriptomic characteristics of bronchoalveolar lavage fluid and peripheral blood mononuclear cells in COVID-19 patients. Emerging microbes & infections. 2020; 9:761–770. DOI: 10.1080/22221751.2020.1747363 [PubMed: 32228226]
35. Dobin A, et al. STAR: ultrafast universal RNA-seq aligner. Bioinformatics. 2013; 29:15–21. DOI: 10.1093/bioinformatics/bts635 [PubMed: 23104886]
36. Liao Y, Smyth GK, Shi W. featureCounts: an efficient general purpose program for assigning sequence reads to genomic features. Bioinformatics. 2014; 30:923–930. DOI: 10.1093/bioinformatics/btt656 [PubMed: 24227677]
37. Johnson WE, Li C, Rabinovic A. Adjusting batch effects in microarray expression data using empirical Bayes methods. Biostatistics. 2007; 8:118–127. DOI: 10.1093/biostatistics/kxj037 [PubMed: 16632515]
38. Love MI, Huber W, Anders S. Moderated estimation of fold change and dispersion for RNA-seq data with DESeq2. Genome biology. 2014; 15:550.doi: 10.1186/s13059-014-0550-8 [PubMed: 25516281]
39. Korsunsky I, et al. Fast, sensitive and accurate integration of single-cell data with Harmony. Nature methods. 2019; 16:1289–1296. DOI: 10.1038/s41592-019-0619-0 [PubMed: 31740819]

Europe PMC Funders Author Manuscripts

Europe PMC Funders Author Manuscripts

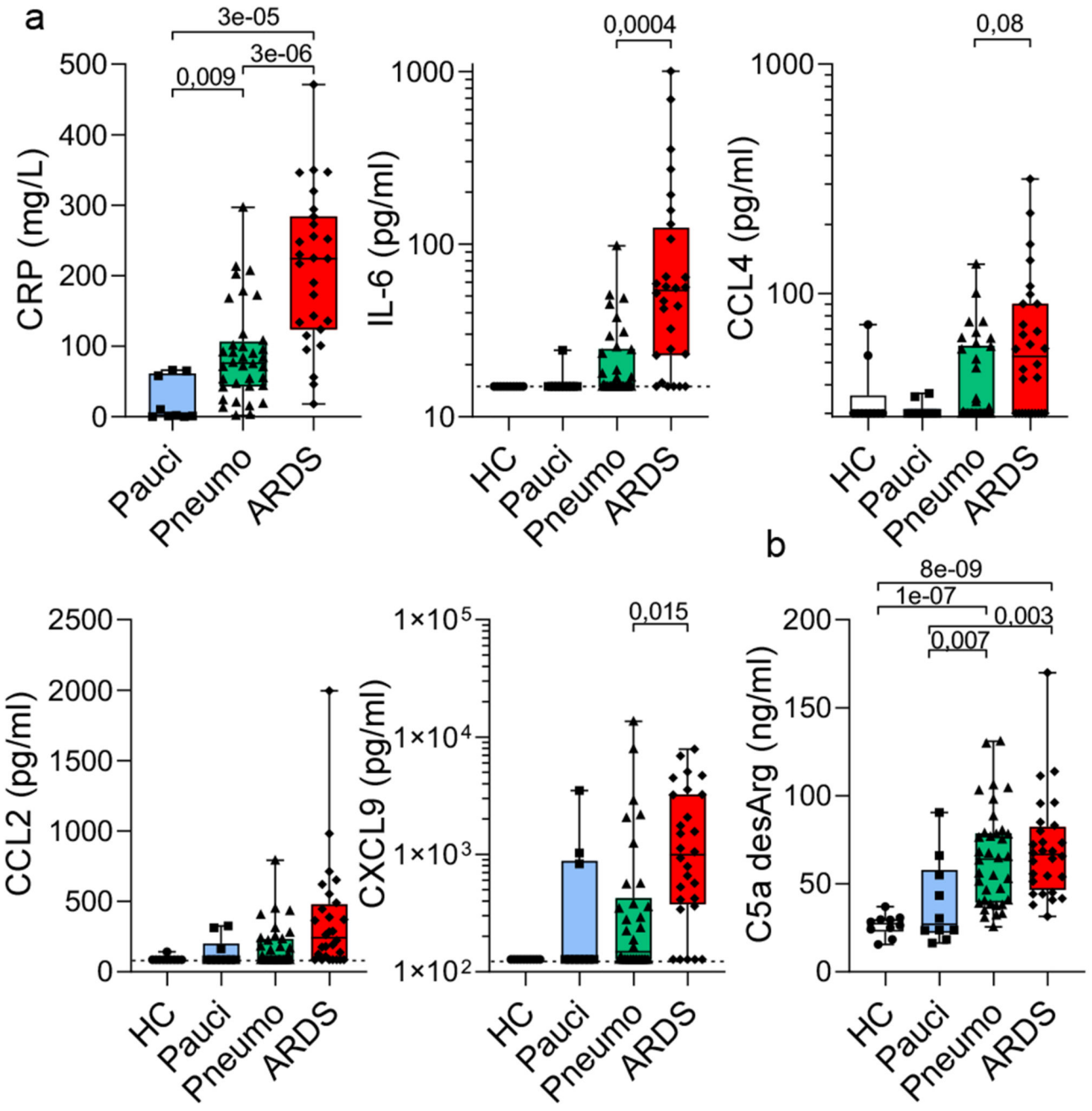

Fig. 1. Inflammation is associated with a cytokine storm and C5a production in COVID-19 patients.

a, Concentrations of CRP, IL-6, CCL4, CCL2 and CXCL9 in plasma from healthy donors (HC) and COVID-19 patients. **b**, Concentration of C5a desArg in plasma of HC and COVID-19 patients. **a-b,** HC (white, *n*=10), pauci (blue, *n*=10), pneumo (green, *n*=31 to 34) and ARDS (red, *n*=26 to 28). For CRP and **b** *p*-values were computed using two-tailed Wilcoxon rank-sum tests. For IL-6, CCL4, CCL2 and CXCL9: a global comparison was first performed in which all values were classified into two categories: above or below the LOQ

(*p*-values for two-sided Fisher's exact tests demonstrated an increase in the number of values above the LOQ with increasing severity); Fisher tests: 5×10^{-7} for IL-6, 0.02 for CCL4, 0.001 for CCL2, 9×10^{-6} for CXCL9. A comparison was then performed between pneumonia and ARDS groups, exclusively for values above the LOQ (*p*-values were computed using two-tailed Wilcoxon rank-sum tests). Each symbol represents a single donor. Boxplots represent the median and 25th to 75th percentiles and the whiskers denote the maximum and minimum values.

Europe PMC Funders Author Manuscripts

Europe PMC Funders Author Manuscripts

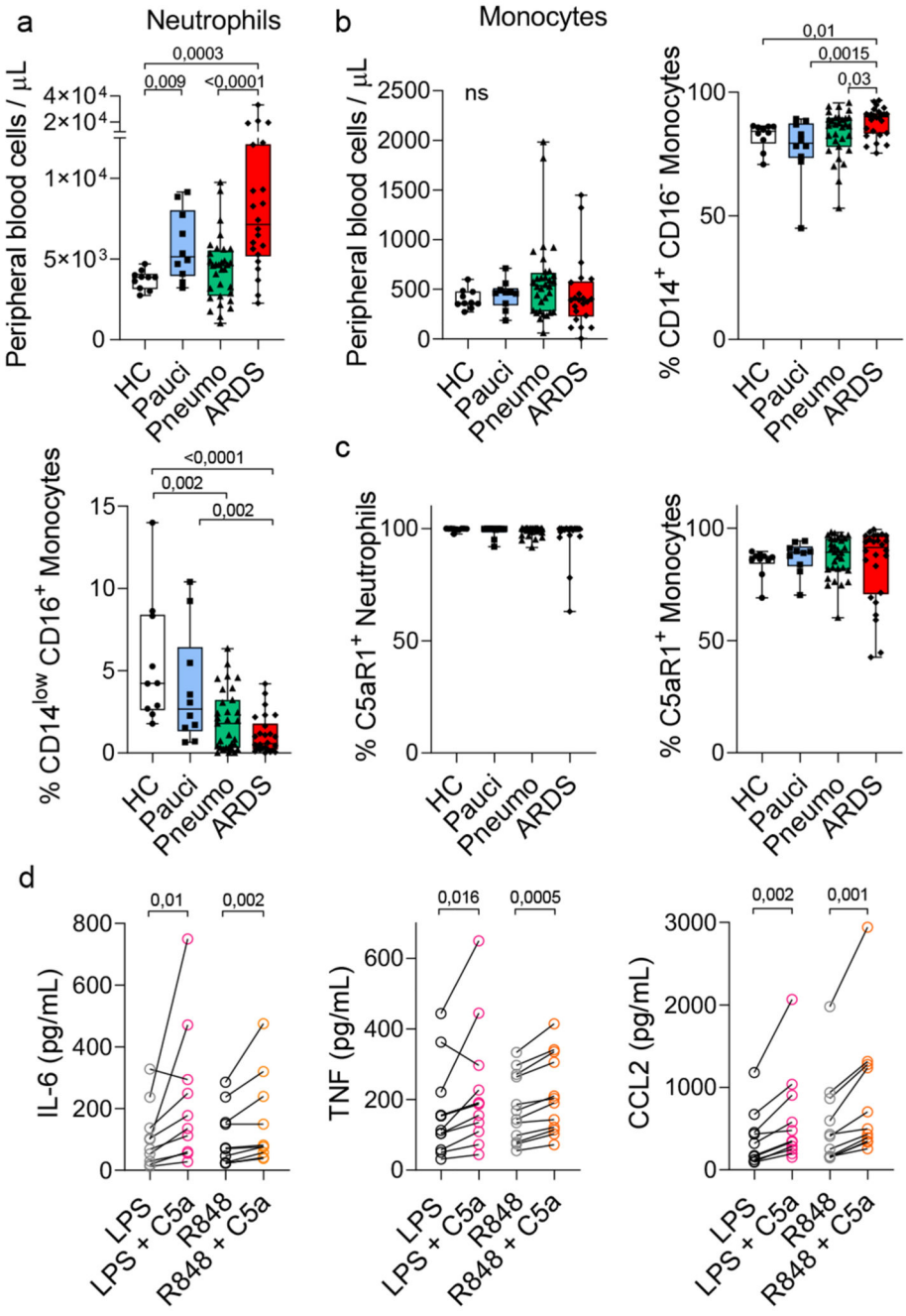

Fig. 2. C5aR1 is highly expressed on myeloid cells and promotes inflammation.

a, Absolute numbers of circulating neutrophils per µL of peripheral blood from healthy donors and COVID-19 patients at T0. **b**, Absolute numbers of circulating total monocytes, and percentages of $CD14^{+}CD16^{-}$ conventional monocytes and $CD14^{low}CD16^{+}$ inflammatory monocytes in the peripheral blood of healthy donors and COVID-19 patients at T0. **c,** Percentage of $C5aR1^{+}$ neutrophils and monocytes in peripheral blood. **a-c**, HC (healthy controls, white, *n*=10), pauci (paucisymptomatic, blue, *n*=10), pneumo (pneumonia, green, *n*=31) and ARDS (red, *n*=26); Each symbol represents a single donor. **d**, IL-6, TNF

and CCL2 production by monocytes purified from PBMCs from COVID-19 patients and activated overnight with LPS (0.5 ng/mL) or R848 (50 ng/mL) and C5a (1 μg/mL), when indicated. Each dot represents the mean value obtained from duplicate or triplicate analyses for a single patient (n=12 patients). Boxplots represent the median and 25th to 75th percentiles and the whiskers denote the maximum and minimum values. The p-values were obtained using two-tailed Wilcoxon rank-sum tests for **a-c** and two-tailed Wilcoxon signed-rank tests for **d.**

Europe PMC Funders Author Manuscripts

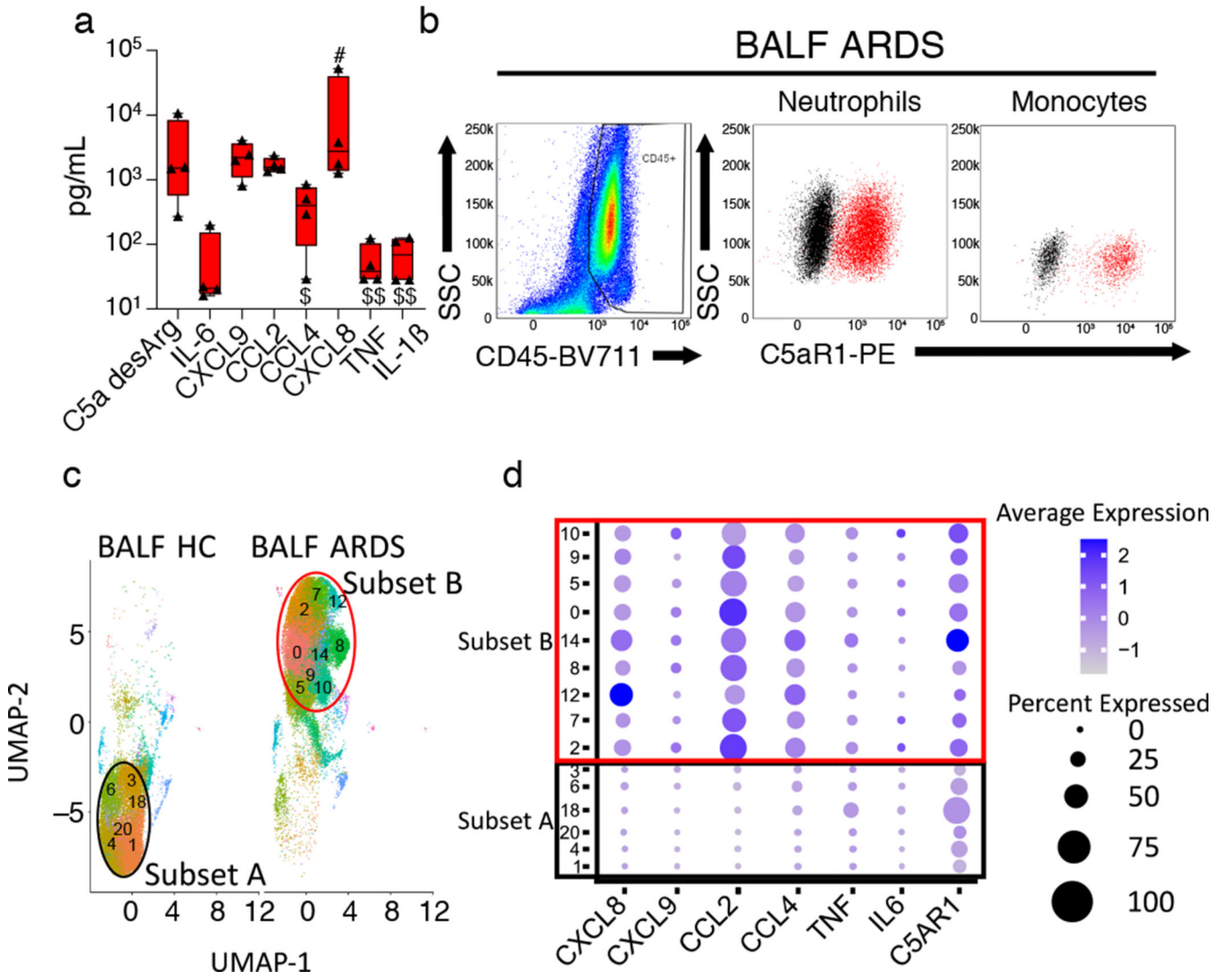

Fig. 3. C5aR1^{+} cells and C5a are detected in lung samples from COVID-19 patients.

a, Concentration of C5a desArg and IL-6, CXCL9, CCL2, CCL4, IL-8, TNF and IL-1β in the BALF of ARDS patients (n=4). # above the detection limit of 52200 pg/mL; $ below the detection limit of 29 pg/mL. **b**, CD45^{+} immune cell infiltration in BALF from ARDS patients visualized by flow cytometry, and C5aR1 expression (red) vs. FMO (black) staining on CD45^{+}CD14^{-}CD15^{+}CD16^{+} neutrophils and CD45^{+}CD33^{+}HLADR^{+}CD14^{+} monocytes in BALF from ARDS patients. The images shown are representative of analyses performed on samples from three ARDS patients. **c**, UMAP of myeloid cell clusters by patient group: healthy controls (n=3) and patients with severe COVID-19 (n=6). **d**, Dotplot of pro-inflammatory cytokine expression, by cluster.

Europe PMC Funders Author Manuscripts

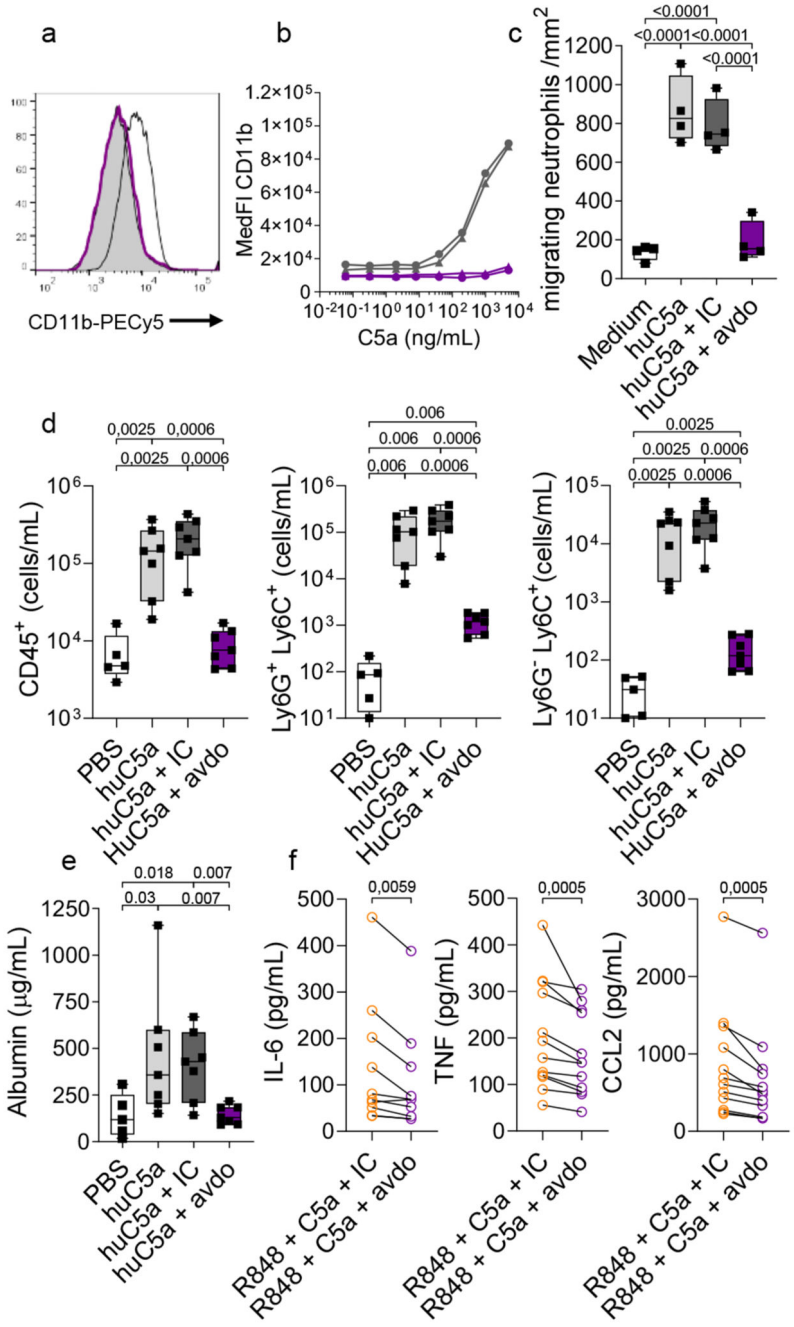

Fig. 4. Targeting C5aR1 blocks C5a-mediated myeloid cell activation and migration.

a, Representative flow cytometry histogram of C5a-mediated CD11b upregulation on whole blood neutrophils, inhibited by avdoralimab. The gray line corresponds to non-activated neutrophils; black line corresponds to C5a-activated neutrophils and purple line corresponds to avdoralimab (30 μg/mL)-treated neutrophils activated with C5a. **b**, CD11b induction through a dose-dependent response to C5a on untreated (gray) or avdoralimab (10 μg/mL)-treated whole-blood neutrophils (purple). Data were obtained from two independent donors. **c**, Migrating neutrophils attracted by C5a. Neutrophils were treated with 10 μg/mL isotype

Europe PMC Funders Author Manuscripts

control (dark gray) or avdoralimab (purple) before the induction of migration. Data for neutrophils purified from four healthy donors are shown. **d-e**, BALF was collected from huC5aR1 knock-in mice 18 hours after intranasal instillation of recombinant human C5a. Mice were pretreated with avdoralimab (avdo, purple) or isotype control (IC, dark gray), when indicated. Each symbol represents data from a single mouse, n=5 for PBS group and n=7 for the other groups. Data are representative of 2 experiments. **d**, BALF cell analysis by flow cytometry including $CD45^+$ immune cells, $Ly6C^+Ly6G^+$ neutrophils and $Ly6C^+Ly6G^-$ monocytes. **e**, Albumin concentration in BALF. **f**, Production of IL-6, TNF and CCL2 by monocytes purified from the PBMCs of COVID-19 patients activated by overnight incubation with R848 (50 ng/mL) and C5a (1 μg/mL). Before activation, monocytes were incubated with 20 μg/mL avdoralimab (avdo) or isotype control (IC). Each dot represents the mean value obtained from duplicate or triplicate analyses of a single donor, n=10 for IL-6 and n=12 for TNF and CCL2. Boxplots represent the median and 25th to 75th percentiles and the whiskers denote the maximum and minimum values. The p-values were computed using paired one-way ANOVA for **c,** two-tailed Wilcoxon rank-sum tests for **d-e** and two-tailed Wilcoxon signed-rank tests for **f**.